

# Heom.jl: An efficient Julia framework for hierarchical equations of motion in open quantum systems

Yi-Te Huang,<sup>1,2,\*</sup> Po-Chen Kuo,<sup>1,2,3,\*</sup> Neill Lambert,<sup>3,†</sup> Mauro Cirio,<sup>4,‡</sup>  
Simon Cross,<sup>3</sup> Shen-Liang Yang,<sup>1,2</sup> Franco Nori,<sup>3,5,6</sup> and Yueh-Nan Chen<sup>1,2,§</sup>

<sup>1</sup>*Department of Physics, National Cheng Kung University, 701 Tainan, Taiwan*

<sup>2</sup>*Center for Quantum Frontiers of Research and Technology, NCKU, 70101 Tainan, Taiwan*

<sup>3</sup>*Theoretical Quantum Physics Laboratory, Cluster for Pioneering Research, RIKEN, Wakoshi, Saitama 351-0198, Japan*

<sup>4</sup>*Graduate School of China Academy of Engineering Physics, Haidian District, Beijing, 100193, China*

<sup>5</sup>*Center for Quantum Computing (RQC), RIKEN, Wakoshi, Saitama 351-0198, Japan*

<sup>6</sup>*Physics Department, The University of Michigan, Ann Arbor, Michigan 48109-1040, USA.*

We introduce an open-source software package called "Heom.jl", a Julia framework to integrate the hierarchical equations of motion (HEOM) for the reduced dynamics of a system simultaneously coupled to multiple bosonic and fermionic environments. Heom.jl features a collection of methods to compute bosonic and fermionic spectra, stationary states, and the full dynamics in the extended space of all auxiliary density operators (ADOs). The required handling of the ADOs multi-indexes is achieved through a user-friendly interface. We exemplify the functionalities of the package by analyzing a single impurity interacting with two fermionic reservoirs (Anderson model), and an ultra-strongly coupled charge-cavity system interacting with one bosonic and two fermionic reservoirs. Heom.jl allows for an order of magnitude speedup in the construction of the HEOM Liouvillian superoperator, solving dynamics and stationary states for all ADOs, with respect to the corresponding method in the Quantum Toolbox in Python (QuTiP), upon which this package is founded.

## INTRODUCTION

The time evolution of a closed quantum system can offer important insights about its nature and properties. However, the dynamics are inevitably affected by interactions with external environments [1, 2], which can involve the exchange of energy or particles, and the suppression of quantum coherence. Due to the effective continuum of degrees of freedom present in these external baths [3, 4], modeling the dynamics of an open quantum system can be challenging. This is especially the case when perturbative approaches [5] are no longer valid due to non-Markovian effects emerging in the presence of strong interaction with the bath [6, 7]. In this regime, standard Markovian master equations are no longer applicable, and non-perturbative techniques are required [8–12].

In particular, here we consider the hierarchical equations of motion (HEOM) approach, which offers a non-perturbative [13] characterization of all the environmental effects on the system. This is achieved by using a hierarchy of auxiliary density operators (ADOs) to model system-bath correlations and entanglement [14, 15]. This makes the HEOM suitable for studying complex systems strongly coupled to either bosonic (with applications in quantum biology [16, 17], quantum optics [18], quantum thermodynamics [19], and quantum information [20]), or fermionic environments (for the analysis of quantum transport [21–23] and condensed matter physics [24]). Additionally, quantum systems interacting simultaneously with both bosonic and fermionic environments can be found in the study of electron transport through both natural and artificial molecules [25, 26]. Naturally, such an increase in the complexity of the environment leads to an increase in computational resources which, in the case of the HEOM method, corresponds to an increase in the size of the HEOM Liouvillian superoperator (HEOMLS) matrix. To deal with this issue, it is beneficial to explore the numerical efficiency of programming languages designed to optimize different computational resources.

In this work, we use `Julia` [27, 28]: a dynamic general-purpose, high-level programming language capable of high-performance in scientific applications. It was created in 2012 with the goal to build a language with the speed of C [29], the dynamism of Ruby [30], the practicality of Python [31], and able to solve statistics and linear algebra tasks like R [32] and Matlab [33], respectively. `Julia` is extremely fast because it uses a just-in-time compiler [34] to convert source code into machine code before running it. Recently, many researchers are turning to `Julia` to build high-performance simulations and models for open quantum system dynamics [35], quantum optics [36], quantum algorithms [37] and quantum information theories [38]. Moreover, the variable name in `Julia` supports UTF-8 encoding (e.g., Greek symbols and mathematical symbols) which allows to write equations in code more elegantly.

\* These authors contributed equally.

† [nwlambert@gmail.com](mailto:nwlambert@gmail.com)

‡ [cirio.mauro@gmail.com](mailto:cirio.mauro@gmail.com)

§ [yuehnan@mail.ncku.edu.tw](mailto:yuehnan@mail.ncku.edu.tw)

`Heom.jl` is developed following the `Julia` design philosophy: one can have machine performance without sacrificing human convenience [27]. The entire ecosystem of `Heom.jl` package is summarized in Fig. 1. The following innovative characteristics define the package:

- It significantly decreases the number of ADOs and the size of the HEOMLS matrix by allowing the user to specify *importance* thresholds [23, 39].
- It provides built-in functions to calculate the spectrum for both bosonic and fermionic systems based on `LinearSolve.jl` [40].
- It provides a dictionary translating the index of the ADOs to the corresponding bath exponential-expansion series, and vice versa. This allows an easy way to interrogate the ADOs to gain access to bath properties, like electronic and heat currents.
- User can choose to construct the HEOMLS matrices within even- or odd-parity for fermionic baths. It depends on the parity of the operator which the HEOMLS matrix is acting on.
- It provides built-in functions for the user to further add Lindbladians to the HEOMLS matrices while keeping the size of HEOMLS matrix unchanged (it does not extend the ADO space). The Lindbladian describes the dissipative interaction (under Born-Markov approximation [41]) between the system and extra environments.

Moreover, `Heom.jl` also takes advantage of other available packages for the following features:

- It is written in `Julia`.
- It supports different choices of spectral densities and spectral decomposition methods to accurately compute bath correlation functions.
- It supports time-dependent system Hamiltonians.
- It constructs the HEOMLS matrix for different types (bosonic, fermionic, or hybrid) of baths.
- The HEOMLS matrix is constructed using multi-threading.
- It provides different methods based on `DifferentialEquations.jl` [42], `LinearSolve.jl` [40], and `FastExpm.jl` [43] to compute the dynamics and stationary states of all ADOs.

## RESULTS

### Preliminaries for hierarchical equations of motion

Throughout this work, we consider an open quantum system (s) interacting with *fermionic* (f) and *bosonic* (b) environments described by the following total (T) Hamiltonian ( $\hbar$  is set to unity throughout this work):

$$H_T = H_s(t) + H_f + H_b + H_{sf} + H_{sb}, \quad (1)$$

where  $H_s(t)$  is the (possibly time-dependent) system Hamiltonian containing boson and fermion particles. Here, we allow the fermionic environment to be composed by multiple baths of non-interacting fermionic degrees of freedom described by the Hamiltonian

$$H_f = \sum_{\alpha} \sum_k \epsilon_{\alpha,k} c_{\alpha,k}^\dagger c_{\alpha,k}, \quad (2)$$

where  $c_{\alpha,k}$  ( $c_{\alpha,k}^\dagger$ ) annihilates (creates) a fermion (f) in the state  $k$  (with energy  $\epsilon_{\alpha,k}$ ) of the  $\alpha$ th fermionic bath. Analogously,

$$H_b = \sum_{\beta} \sum_k \omega_{\beta,k} b_{\beta,k}^\dagger b_{\beta,k}, \quad (3)$$

describes a generic bosonic environment which can accommodate multiple non-interacting bosonic baths in which  $b_{\beta,k}$  ( $b_{\beta,k}^\dagger$ ) is the bosonic creation (annihilation) operator associated to the  $k$ th mode (with frequency  $\omega_{\beta,k}$ ) in the  $\beta$ th bosonic bath. This bosonic environment can represent a broad range of physical environments, e.g., electromagnetic environments [44, 45], phonon environments [46–48], surface plasmon modes [49, 50] and vibronic environments in molecules (e.g., nuclear motion in a

photosynthetic complex [22]). The interaction Hamiltonian between a fermionic system and the *fermionic environments* can be written as

$$H_{\text{sf}} = \sum_{\alpha,k} \left( g_{\alpha,k} c_{\alpha,k}^\dagger d_s + g_{\alpha,k}^* d_s^\dagger c_{\alpha,k} \right), \quad (4)$$

in terms of the *coupling strengths*  $g_{\alpha,k}$ . Analogously, the interaction between a bosonic or fermionic system and the exterior *bosonic environments* can be modeled by

$$H_{\text{sb}} = V_s \sum_{\beta,k} g_{\beta,k} (b_{\beta,k} + b_{\beta,k}^\dagger), \quad (5)$$

in terms of the coupling strengths  $g_{\beta,k}$ . Note that  $d_s$  and  $V_s$  refer to the system-interaction operators. In particular,  $d_s$  is an odd-parity operator destroying a fermion in the system, while  $V_s$  is a Hermitian operator which can act on both fermionic and bosonic degrees of freedom. In the fermionic case,  $V_s$  must have even parity to be compatible with charge conservation.

Without resorting to any approximation, the reduced density matrix for the system at time  $t$  can be written in terms of the following Dyson series

$$\tilde{\rho}_s(t) = \hat{\mathcal{G}}(t) [\rho_s^p(0)], \quad (6)$$

where  $\hat{\mathcal{G}}(t)[\cdot]$  is a *canonical superoperator* [51] which propagates the even- ( $p = +$ ) or odd-parity ( $p = -$ ) density operator initially in the state  $\rho_s^p(0)$ . This operator takes the form

$$\hat{\mathcal{G}}(t)[\cdot] = \hat{\mathcal{T}} \exp \left\{ - \int_0^t dt_1 \int_0^{t_1} dt_2 \left[ \hat{\mathcal{W}}_f(t_1, t_2)[\cdot] + \hat{\mathcal{W}}_b(t_1, t_2)[\cdot] \right] \right\}, \quad (7)$$

in terms of the time-ordering operator  $\hat{\mathcal{T}}$ , together with fermionic [51] and bosonic [15, 16] operators explicitly written as

$$\hat{\mathcal{W}}_f(t_1, t_2)[\cdot] = \sum_{\alpha} \sum_{p=\pm} \sum_{v=\pm 1} \left\{ C_{\alpha}^v(t_1, t_2) \left[ d_s^{\bar{v}}(t_2), d_s^v(t_1) \cdot \right]_{-p} + C_{\alpha}^v(t_2, t_1) \left[ \cdot d_s^{\bar{v}}(t_2), d_s^v(t_1) \right]_{-p} \right\}, \quad (8)$$

and

$$\hat{\mathcal{W}}_b(t_1, t_2)[\cdot] = \sum_{\beta} \left[ V_s(t_1), \left( C_{\beta}^{\mathbb{R}}(t_1, t_2) [V_s(t_2), \cdot]_{-} + i C_{\beta}^{\mathbb{I}}(t_1, t_2) [V_s(t_2), \cdot]_{+} \right) \right]_{-}, \quad (9)$$

respectively. Here,  $p = \mp$  represents the projection on the even or odd parity sector, while  $[\cdot, \cdot]_{-}$  and  $[\cdot, \cdot]_{+}$  denote the commutator and anticommutator, respectively. For simplicity, we define  $v$  to denote the presence ( $v = +1$ ) or absence ( $v = -1$ ) of a Hermitian conjugation and  $\bar{v} := -v$ .

As it can be seen from the expressions above, the effects of fermionic and bosonic environments (initially in thermal equilibrium and linearly coupled to a system) are completely encoded in the two-time correlation functions. In the fermionic case, they depend on the spectral density  $J_{\alpha}(\omega) = 2\pi \sum_k |g_{\alpha,k}|^2 \delta(\omega - \omega_k)$  and the Fermi–Dirac distribution  $n_{\alpha}^{\text{eq}}(\omega) = \{\exp[(\omega - \mu_{\alpha})/k_B T_{\alpha}] + 1\}^{-1}$  as

$$C_{\alpha}^v(t_1, t_2) = \frac{1}{2\pi} \int_{-\infty}^{\infty} d\omega J_{\alpha}(\omega) \left[ \frac{1-v}{2} + v n_{\alpha}^{\text{eq}}(\omega) \right] e^{v i \omega (t_1 - t_2)}. \quad (10)$$

Analogously, in the bosonic case, they depend on the spectral density  $J_{\beta}(\omega) = 2\pi \sum_k g_{\beta,k}^2 \delta(\omega - \omega_k)$  and the Bose–Einstein distribution  $n_{\beta}^{\text{eq}}(\omega) = \{\exp[\omega/k_B T_{\beta}] - 1\}^{-1}$  as

$$C_{\beta}(t_1, t_2) = \frac{1}{2\pi} \int_0^{\infty} d\omega J_{\beta}(\omega) \left[ n_{\beta}^{\text{eq}}(\omega) e^{i \omega (t_1 - t_2)} + (n_{\beta}^{\text{eq}}(\omega) + 1) e^{-i \omega (t_1 - t_2)} \right], \quad (11)$$

where  $k_B$  is the Boltzmann constant and  $T_{\alpha}$  ( $T_{\beta}$ ) represents the absolute temperature of the  $\alpha$ -fermionic ( $\beta$ -bosonic) bath. A non-zero chemical potential ( $\mu_{\alpha} \neq 0$ ) in the  $\alpha$ -fermionic bath can account for non-equilibrium physics.

A more practical representation of Eq. (6) can be found by expressing the bath *correlation functions*  $C(t_1, t_2)$  as a sum of exponential terms (exponents). This allows to define an iterative procedure which leads to the celebrated hierarchical equations of motion (HEOM). Specifically, different approaches, such as the Matsubara [52] or the Padé [53] spectral decompositions, can be used (see Methods) to write the fermionic and bosonic correlation functions as, respectively,

$$C_{\alpha}^v(\tau) = \sum_{h=1}^{N_{\alpha}} \eta_{\alpha,h}^v \exp(-\gamma_{\alpha,h}^v \tau), \quad (12)$$

and

$$C_\beta(\tau) = \sum_{l=1}^{N_\beta} \xi_{\beta,l} \exp(-\chi_{\beta,l}\tau), \quad (13)$$

where  $\tau = t_1 - t_2$ , and  $N_\alpha$  ( $N_\beta$ ) is the total number of exponentials for the  $\alpha$ -fermionic ( $\beta$ -bosonic) bath. When  $\chi_{\beta,l} \neq \chi_{\beta,l}^*$ , a closed form for the HEOM can be obtained by further decomposing the bosonic correlation function into its real ( $\mathbb{R}$ ) and imaginary ( $\mathbb{I}$ ) parts as

$$C_\beta(\tau) = \sum_{u=\mathbb{R},\mathbb{I}} (\delta_{u,\mathbb{R}} + i\delta_{u,\mathbb{I}}) C_\beta^u(\tau) \quad (14)$$

where  $\delta$  is the Kronecker delta function and where

$$C_\beta^u(\tau) = \sum_{l=1}^{N_\beta^u} \xi_{\beta,l}^u \exp(-\chi_{\beta,l}^u\tau). \quad (15)$$

The expressions for the fermionic [Eq. (12)] and bosonic [Eq. (14)] correlation functions can now be used in Eq. (7). The resulting expression can be recursively differentiated in time [18, 51, 54] to define a local master equation in an enlarged space made out of *auxiliary density operators* (ADOs)  $\rho_{\mathbf{j}|\mathbf{q}}^{(m,n,p)}(t)$ . Intuitively, these variables encode environmental effects related to different exponential terms present in the correlation function and provide an iterative description of high-order system-baths memory effects. In  $\rho_{\mathbf{j}|\mathbf{q}}^{(m,n,p)}(t)$ , the tuple  $(m,n,p)$  represents the  $m$ th-level-bosonic-and- $n$ th-level-fermionic ADO with parity  $p$ , and  $\mathbf{j}$  ( $\mathbf{q}$ ) denotes a vector  $[j_m, \dots, j_1]$  ( $[q_n, \dots, q_1]$ ), where each  $j$  ( $q$ ) represents a specific multi-index ensemble  $\{\beta, u, l, \sigma_b\}$  ( $\{\alpha, v, h, \sigma_f\}$ ). The indexes  $\sigma_b$  and  $\sigma_f$  are used to specify other quantum numbers (such as energy or spin) of the system interacting with a bosonic or fermionic bath, respectively. In this way, the hierarchical equations of motion in the Schrödinger picture can be expressed as

$$\begin{aligned} \partial_t \rho_{\mathbf{j}|\mathbf{q}}^{(m,n,p)}(t) &\equiv \hat{\mathcal{M}} \rho_{\mathbf{j}|\mathbf{q}}^{(m,n,p)}(t) \\ &= - \left( i\hat{\mathcal{L}}_s + \sum_{r=1}^m \chi_{j_r} + \sum_{w=1}^n \gamma_{q_w} \right) \rho_{\mathbf{j}|\mathbf{q}}^{(m,n,p)}(t) \\ &\quad - i \sum_{q' \notin \mathbf{q}} \hat{\mathcal{A}}_{q'} \rho_{\mathbf{j}|\mathbf{q}^+}^{(m,n+1,p)}(t) - i \sum_{j'} \hat{\mathcal{B}}_{j'} \rho_{\mathbf{j}^+|\mathbf{q}}^{(m+1,n,p)}(t) \\ &\quad - i \sum_{w=1}^n (-1)^{n-w} \hat{\mathcal{C}}_{q_w} \rho_{\mathbf{j}|\mathbf{q}_w^-}^{(m,n-1,p)}(t) - i \sum_{r=1}^m \hat{\mathcal{D}}_{j_r} \rho_{\mathbf{j}_r^-|\mathbf{q}}^{(m-1,n,p)}(t), \end{aligned} \quad (16)$$

where we used the multi-index notation:

$$\begin{aligned} \mathbf{j}^+ &= [j', j_m, \dots, j_1], \\ \mathbf{q}^+ &= [q', q_n, \dots, q_1], \\ \mathbf{j}_r^- &= [j_m, \dots, j_{r+1}, j_{r-1}, \dots, j_1], \\ \mathbf{q}_w^- &= [q_n, \dots, q_{w+1}, q_{w-1}, \dots, q_1]. \end{aligned} \quad (17)$$

Here,  $j'$  can be chosen from any one of the elements in  $\mathbf{j}$  or any other bosonic multi-index ensemble that has not yet be considered in  $\mathbf{j}$ , whereas  $q' \notin \mathbf{q}$  due to the Pauli exclusion principle.

Furthermore, we defined  $\mathcal{L}_s[\cdot] = [H_s(t), \cdot]_-$  characterizing the bare system dynamics. System-bath interactions are encoded by the fermionic superoperators  $\hat{\mathcal{A}}_q$ ,  $\hat{\mathcal{C}}_q$  (to couple the  $n$ th-level-fermionic ADOs to the  $(n+1)$ th-level- and  $(n-1)$ th-level-fermionic ADOs, respectively), and the bosonic superoperators  $\hat{\mathcal{B}}_j$ ,  $\hat{\mathcal{D}}_j$  (to couple the  $m$ th-level-bosonic ADOs to the  $(m+1)$ th-level- and  $(m-1)$ th-level- bosonic ADOs, respectively). Their explicit forms are given by

$$\begin{aligned} \hat{\mathcal{A}}_q[\cdot] &= (-1)^{\delta_{p,-}} \left\{ d_{\sigma_f}^{\bar{v}}[\cdot] - \hat{\mathcal{P}}_s [[\cdot] d_{\sigma_f}^{\bar{v}}] \right\}, \\ \hat{\mathcal{C}}_q[\cdot] &= (-1)^{\delta_{p,-}} \left\{ \eta_{\alpha,h}^v d_{\sigma_f}^v[\cdot] + (\eta_{\alpha,h}^{\bar{v}})^* \hat{\mathcal{P}}_s [[\cdot] d_{\sigma_f}^v] \right\}, \\ \hat{\mathcal{B}}_j[\cdot] &= \left[ V_{\sigma_b}, \cdot \right]_-, \\ \hat{\mathcal{D}}_j[\cdot] &= \delta_{u,\mathbb{R}} \xi_{\beta,l}^{\mathbb{R}} \left[ V_{\sigma_b}, \cdot \right]_- + i \delta_{u,\mathbb{I}} \xi_{\beta,l}^{\mathbb{I}} \left[ V_{\sigma_b}, \cdot \right]_+, \\ \hat{\mathcal{P}}_s \left[ \rho_{\mathbf{j}|\mathbf{q}}^{(m,n,\pm)}(t) d_{\sigma_f}^v \right] &= \mp (-1)^n \rho_{\mathbf{j}|\mathbf{q}}^{(m,n,\pm)}(t) d_{\sigma_f}^v. \end{aligned} \quad (18)$$

The form of the HEOM in Eq. (16) can be applied to initial states with arbitrary parity symmetry. For example,  $\rho^{(0,0,+)}(t)$  and  $\rho^{(0,0,-)}(t)$  are the system reduced density operator with even- and odd-parity, respectively. To project in the different parity system sub-spaces, we introduced the superoperator

$$\hat{\mathcal{P}}_s[\cdot] = \left( \prod_{\sigma_f} \exp[i\pi d_{\sigma_f}^\dagger d_{\sigma_f}] \right) [\cdot] \left( \prod_{\sigma_f} \exp[i\pi d_{\sigma_f}^\dagger d_{\sigma_f}] \right). \quad (19)$$

Overall, the *Liouvillian superoperator* (HEOMLS)  $\hat{\mathcal{M}}$  characterizes the dynamics in the full ADOs space and it can, numerically, be expressed as a matrix. Table I summarizes the explanation of the most relevant symbols used throughout the article.

Symbol	Description
$\sigma_b$	specification of different quantum numbers of the bosonic system
$\sigma_f$	specification of different quantum numbers of the fermionic system
$\beta$	specification of different bosonic baths
$\alpha$	specification of different fermionic baths
$[\cdot, \cdot]_-$	commutator
$[\cdot, \cdot]_+$	anti-commutator
$v \in \{+1, -1\}$	presence (+1) or absence (-1) of Hermitian conjugation
$\bar{v}$	opposite of $v$ : $\bar{v} \equiv -v$
$p \in \{+, -\}$	even- (+) or odd- (-) parity of the fermion operator
$u \in \{\mathbb{R}, \mathbb{I}\}$	Real ( $\mathbb{R}$ ) or imaginary ( $\mathbb{I}$ ) part of bosonic correlation function
$C(t_1, t_2)$	two time correlation function of the bath
$n^{eq}(\omega)$	Fermi-Dirac or Bose-Einstein equilibrium distribution
$J(\omega)$	spectral density of the bath
$\hat{\mathcal{G}}[\cdot]$	superoperator which propagates all ADOs
$\hat{\mathcal{M}}[\cdot]$	HEOM Liouvillian superoperator (matrix)
$\hat{\mathcal{J}}(F)[\cdot]$	Lindbladian superoperator with jump operator $F$
$\rho_{j q}^{(m,n,p)}$	auxiliary density operator (ADO)
$\rho_{ }^{(0,0,+)}$	reduced density operator
$m$	bosonic hierarchy level
$n$	fermionic hierarchy level
$j$	vector of bosonic multi-index ensembles: $[j_m, \dots, j_1]$
$q$	vector of fermionic multi-index ensembles: $[q_n, \dots, q_1]$
$\hat{\mathcal{I}}\left(\rho_{j q}^{(m,n,p)}\right)$	importance value of a given ADO
$\hat{\mathcal{I}}_{th}$	threshold of importance value
$A(\omega)$	spectrum of fermionic system (density of states; DOS)
$S(\omega)$	spectrum of bosonic system (power spectral density; PSD)
$I_\alpha$	electronic current from $\alpha$ -fermionic bath into the system
$G$	conductance

Table I. List of symbols used in this article.

In practice, the dimensions of this matrix must be finite and the hierarchical equations must be truncated at a suitable bosonic-level ( $m_{\max}$ ) and fermionic-level ( $n_{\max}$ ). Previous works [23, 55] showed that the computational effort can be optimized by associating an *importance value* to each ADO and then discarding all ADOs (in the second and higher levels) whose importance value is smaller than a threshold value  $\mathcal{I}_{th}$ . The importance value  $\mathcal{I}$  for a given ADO  $\rho_{j|q}^{(m,n,p)}$  is defined as

$$\mathcal{I}\left(\rho_{j|q}^{(m,n,p)}\right) = \left| \prod_{r=1}^m \left( \frac{\xi_{j_r}}{\text{Re}[\chi_{j_r}] \sum_{x=1}^r \text{Re}[\chi_{j_x}]} \right) \right| \times \left| \prod_{w=1}^n \left( \frac{\eta_{q_w}}{\text{Re}[\gamma_{q_w}] \sum_{x=1}^w \text{Re}[\gamma_{q_x}]} \right) \right|, \quad (20)$$

where the first and second absolute value represents the “importance” of the bosonic part [26] and fermionic part [56] of the hierarchy, respectively. Note that for hybrid (consider bosonic and fermionic baths at the same time) cases, we retain all the

ADOs where their hierarchy levels  $(m, n) \in \{(0, 0), (0, 1), (1, 0), (1, 1)\}$ , and all the other high-level ADOs may be neglected if their importance value is less than  $\mathcal{I}_{\text{th}}$ . Moreover, the full hierarchical equations can be recovered in the limiting case  $\mathcal{I}_{\text{th}} \rightarrow 0$ . We will provide a concrete example and detailed discussion later.

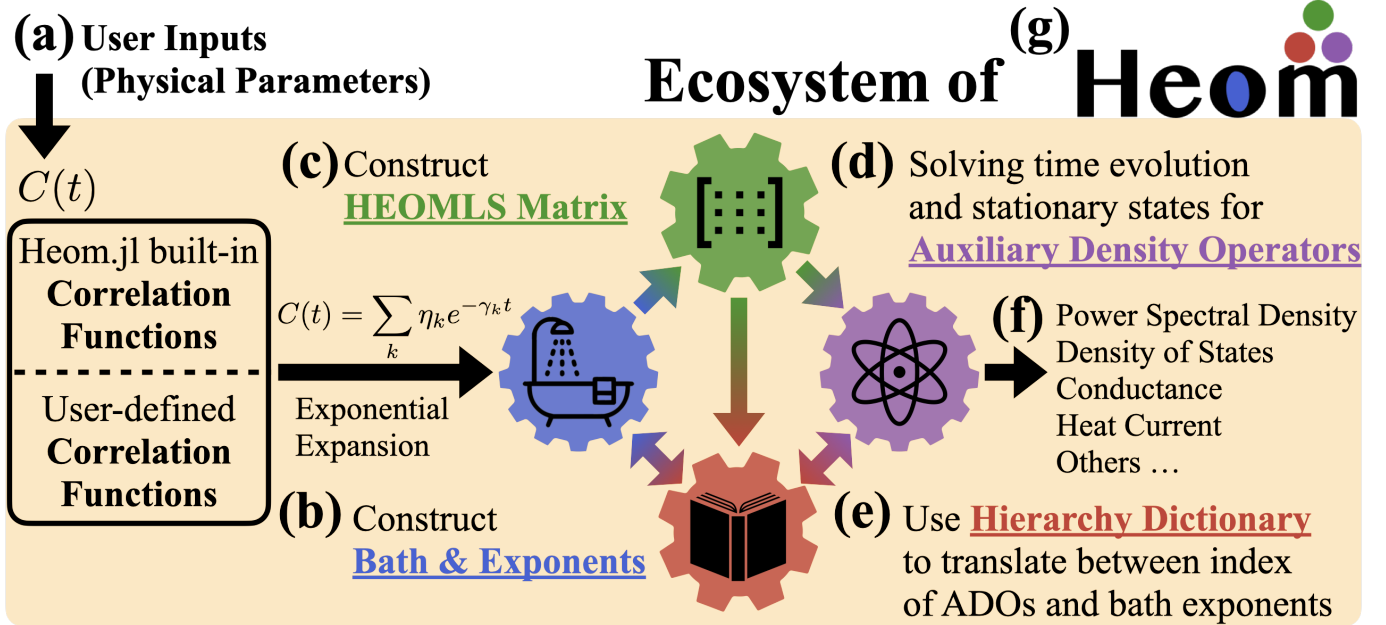


Figure 1. **The ecosystem of the Heom.jl package.** (a) Users can input bath correlation functions either by specifying the physical parameters characterizing their spectral densities or by directly providing a list of exponents. (b) Construction of the bath-object which includes the system coupling operator and a list of exponents characterizing the bath correlation function. (c) Construction of the HEOM Liouvillian superoperator matrix  $\hat{M}$  which defines the hierarchical equations of motion from the system Hamiltonian and the bath-objects. (d) Computation of the dynamics and stationary states for all auxiliary density operators using  $\hat{M}$ . (e) The hierarchy dictionary translates the index of each ADO into the corresponding multi-index ensembles together with the exponents of the bath, and vice-versa. (f) The hierarchy dictionary allows a high-level interpretation of the ADOs to compute some physical properties. (g) Logo of Heom.jl package.

#### Package architecture and design philosophy

The package Heom.jl is designed to integrate the efficiency of Julia with the functionalities provided by other existing HEOM packages [15, 24, 57–59]. This leads to an intuitive interface to construct arbitrary Hamiltonians and initial states (which can be accomplished directly with the built-in library for linear algebra in Julia or by taking advantage of the package QuantumOptics.jl [36]). We now introduce the ecosystem of the package as summarized in Fig. 1.

Following Fig. 1(a) and Fig. 1(b), users can specify the bath correlation functions in Eq. (10) and Eq. (11) by an exponential series as shown in Eqs. (12–15). Heom.jl provides built-in functions to construct these series from physical parameters (e.g., coupling operator, coupling strength, temperature, etc.). For example, it is possible to choose between a Drude-Lorentz and a Lorentzian spectral density for bosonic baths and a Lorentzian spectral density for fermionic baths. For each of these cases, the correlations are computed using either the Matsubara [52] or Padé spectral decomposition [53].

Alternatively, Heom.jl offers the possibility to manually define the correlation functions (simply supplying the coupling operator and the list of exponents). Additional spectral densities could be incorporated into the built-in functions in future releases. We explicitly note that the package allows for any combination of fermionic and bosonic baths.

After the definition of the bath, users can further specify the system Hamiltonian  $H_s(t)$  and consequently construct the HEOMLS matrix  $\hat{M}$  in Eq. (16), see Fig. 1(c). At this stage, Heom.jl offers the possibility to optimize this matrix by neglecting all the ADOs (at second or higher order) whose importance values in Eq. (20) are below the user-specified threshold  $\mathcal{I}_{\text{th}}$ . For fermionic baths, it is also possible to choose the even- or odd-parity of  $\hat{M}$  (see the Methods section: Numerical Computation of the Spectrum). Moreover, our package allows users to further add a *Lindbladian* (superoperator) to  $\hat{M}$ . The Lindbladian describes the dissipative interaction between the system and extra environment while its explicit form is given by

$$\hat{J}(F)[\cdot] = F[\cdot]F^\dagger - \frac{1}{2}[F^\dagger F, \cdot]_+, \quad (21)$$

where  $F$  is the jump operator and describes the dissipation dynamics of the system. Including such Lindbladians when some of the baths are weakly coupled to the system is more efficient than solving the full HEOM since it does not require any ADOs for such baths and hence reduces the size of  $\hat{\mathcal{M}}$  (see Example 2 for more details).

As shown in Fig. 1(d), with this information it is possible to proceed with solving for the dynamics of all the ADOs as described in Eq. (16). `Heom.jl` provides two distinct methods to compute the dynamics. The first one relies on `DifferentialEquations.jl` [42] which provides a set of low-level solvers for ordinary differential equations. The second method directly builds the propagator when the system Hamiltonian is time-independent:  $\hat{\mathcal{G}}(t) = \exp(\hat{\mathcal{M}}t)$  using `FastExpm.jl` [43] which is optimized for the exponentiation of either large-dense or sparse matrices. In addition, `Heom.jl` can also directly solve for the stationary states of all the ADOs using `LinearSolve.jl` [40], which offers a unified interface to solve linear equations in Julia.

To allow further analysis of specific physical properties, `Heom.jl` provides a hierarchy dictionary, as depicted in Fig. 1(e) and Fig. 1(f). This dictionary translates the index of each ADO in terms of the corresponding exponential terms of the bath, and vice-versa. This feature is designed to allow a high-level description of the ADOs, which can be useful in the analysis of electronic currents [21, 23], heat currents [19, 60, 61], and higher-order moments of heat currents [62]. Moreover, `Heom.jl` can calculate the spectrum for both bosonic and fermionic systems using `LinearSolve.jl` (see the Methods section: Numerical computation of the spectrum).

We now demonstrate the use of `Heom.jl` with two examples: a single impurity strongly coupled to fermionic reservoirs and an ultra-strongly coupled charge–cavity system interacting with both bosonic and fermionic reservoirs.

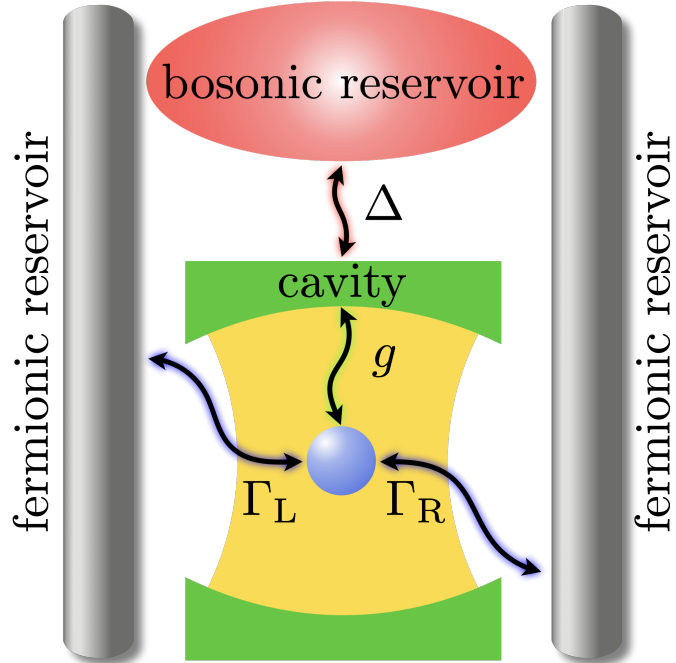


**Figure 2. Schematic illustration of a light-matter system (an electron coupled to a bosonic mode in a cavity) interacting with bosonic and fermionic reservoirs.** Here,  $g$  is the coupling strength between the electron and cavity,  $\Delta$  is the coupling strength between the cavity and the bosonic reservoir, and  $\Gamma_L = \Gamma_R = \Gamma$  are the coupling strengths between the electron and its fermionic reservoirs.

### Example 1: Electronic system strongly interacting with fermionic reservoirs

The investigation of the Kondo effect in electronic systems is crucial as it serves both as a valuable testing ground for the theories of the Kondo effect and has the potential to lead to a better understanding of this intrinsic many-body phenomena [63–65], with applications in building new generation nanoscale electronic devices [66–68] and quantum computation [69]. In this sense, we here consider a single-level electronic system [which can be populated by a spin up,  $\sigma_f = \uparrow$ , or spin down electron,  $\sigma_f = \downarrow$ ] coupled to two [left (L) and right (R)] fermionic reservoirs, as illustrated in Fig. (2). In this case, the different Hamiltonian terms

Example	$\varepsilon$	$U$	$\omega_c$	$g$	$\Gamma$	$\Delta$	$W_\beta$	$W_\alpha$	$e\Phi$	$k_B T$	$N_{\text{photon}}$	$N_\beta$	$N_\alpha$	$m_{\text{max}}$	$n_{\text{max}}$	$\mathcal{I}_{\text{th}}$
(1)	-5	10	$\times$	$\times$	1	$\times$	$\times$	10	[0, 4]	0.5	$\times$	$\times$	7	$\times$	4	$10^{-7}$
(2)	-3	$\times$	1	[0, 0.5]	1	0.01	0.2	10	[0, 10]	0.5	6	5	7	4	3	$10^{-6}$

Table II. **Parameters used in the examples.** Here,  $\varepsilon$  and  $\omega_c$  are, respectively, the energies of the electron state and the frequency of the cavity mode, while  $U$  represents the Coulomb repulsion energy. The electron-cavity, electron-(fermionic reservoir), and cavity-(bosonic reservoir) couplings strengths are specified by  $g$ ,  $\Gamma$ , and  $\Delta$ , respectively.  $W_\beta$  and  $W_\alpha$  are the band-widths of the bosonic and fermionic reservoir, respectively. The bias voltage  $\Phi$  is used to characterize the chemical potential of the fermionic reservoirs as  $\mu_L = -\mu_R = \Phi/2$  (in terms of the elementary charge  $e$ ). All the reservoirs are initially at equilibrium at the same value of  $k_B T$ , where  $k_B$  is the Boltzmann constant and  $T$  is the temperature. Note that all the values are considered in units of milli-electronvolt (meV). The truncation parameters are:  $N_{\text{photon}}$  for the Fock space dimension,  $N_\beta$  for the number of exponential terms for the bosonic reservoirs,  $N_\alpha$  for the number of exponential terms for the fermionic reservoirs,  $m_{\text{max}}$  for the tier of the bosonic hierarchy,  $n_{\text{max}}$  for the tier of the fermionic hierarchy and  $\mathcal{I}_{\text{th}}$  for the importance threshold.

in Eq. (1) take the form

$$H_s = \varepsilon (d_{\uparrow}^\dagger d_{\uparrow} + d_{\downarrow}^\dagger d_{\downarrow}) + U (d_{\uparrow}^\dagger d_{\uparrow} d_{\downarrow}^\dagger d_{\downarrow}),$$

$$H_f = \sum_{\alpha=L,R} \sum_{\sigma_f=\uparrow,\downarrow} \sum_k \varepsilon_{\alpha,\sigma_f,k} c_{\alpha,\sigma_f,k}^\dagger c_{\alpha,\sigma_f,k},$$

$$H_{sf} = \sum_{\alpha=L,R} \sum_{\sigma_f=\uparrow,\downarrow} \sum_k g_{\alpha,k} c_{\alpha,\sigma_f,k}^\dagger d_{\sigma_f} + g_{\alpha,k}^* d_{\sigma_f}^\dagger c_{\alpha,\sigma_f,k},$$

where  $\varepsilon$  is the energy of the impurity and  $U$  is the Coulomb repulsion energy for double occupation. We further assume both fermionic reservoirs to have a Lorentzian-shaped spectral density. As we discussed above, the correlation function in Eq. (10) can be expressed as a sum of exponential terms, see Eq. (12), using the Padé decomposition (see Methods). These spectral densities depend on the following physical parameters: the coupling strength  $\Gamma_L = \Gamma_R = \Gamma$  between system and reservoirs, the band-width  $W_\alpha$ , the temperature  $T$ , and the chemical potential  $\mu_L = -\mu_R = \Phi/2$ , where  $\Phi$  is the bias voltage. We summarize the values of these parameters in Table. II. With these choices, it is now possible to use `Heom.jl` to construct the HEOMLS matrix  $\hat{\mathcal{M}}$  and solve for the stationary states of all the auxiliary density operators (ADOs).

By using the built-in function in `Heom.jl`, we first compute the spectrum of the system (also known as density of states (DOS); see Methods) in the stationary state and plot the results in Fig. 3(a). The DOS of the system exhibits two Hubbard peaks and an additional central peak. The negative frequency Hubbard peak is a consequence of the singly occupied electron state with either spin-up or spin-down. Similarly, double occupation of the state contributes to the resonance at energy  $\varepsilon + U$ . When the system is in equilibrium, the Kondo-resonance central peak is a consequence of the many-body entanglement between the single electron populating the system and the electrons in the fermionic reservoirs. As the bias voltage  $\Phi$  is increased, the central peak splits into two [70]. This ultimately results in two distinct energies for the Kondo cloud which depend on the Fermi-level of the fermionic reservoirs [71, 72].

Alternatively, the Kondo effect can also be probed by calculating the differential conductance  $G = dI/d\Phi$  between the system and fermionic reservoirs. To compute this quantity, we first compute the electronic current in the stationary states of the ADOs (see Methods) as a function of the bias voltage  $\Phi$  and then take the derivative numerically. The zero-bias conductance peak shown in Fig. 3(b) is another manifestation of the existence of a single-channel spin-1/2 Kondo resonance. In fact, in this regime, the system effectively acts as a one-dimensional channel for the moving electrons thereby increasing the conductance [73].

### Example 2: The ultra-strongly coupled charge–cavity system interacting with bosonic and fermionic reservoirs

A crucial aspect of quantum transport research involves investigating impurities, coupled to normal metal contacts, whose charge degree of freedom is strongly coupled to cavity photons[74–76]. By integrating quantum dots with microwave cavities, researchers can investigate such novel “cavity QED” systems[77], yielding insights into a diverse range of quantum phenomena such as out-of-equilibrium state occupation in double quantum dots[78], reservoir-induced charge relaxation in single dots[79], and photo-assisted tunneling processes[74, 80]. Going beyond the strong coupling regime, we here consider a single-level electronic system ultra-strongly coupled to a single-mode cavity [81]. The electronic impurity is in contact with two distinct, left (L) and right (R), fermionic reservoirs, while the cavity is in contact with a bosonic reservoir, as illustrated in Fig. (2). In order to focus on the charge-photon interaction, this model neglects the electronic spin degree of freedom. As a consequence,

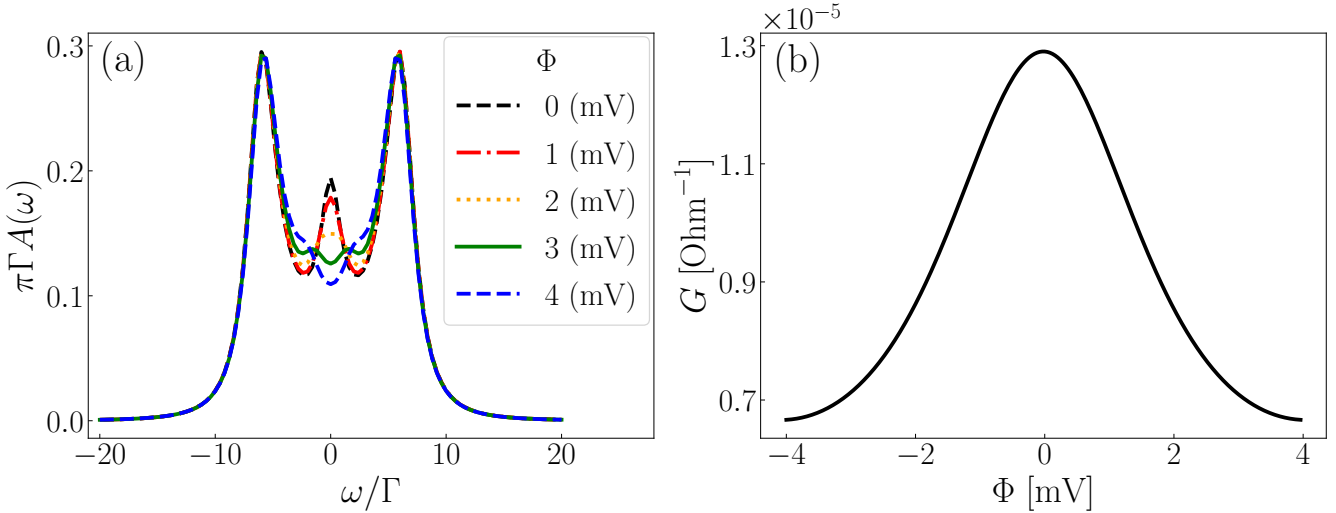


Figure 3. **The Kondo resonance from equilibrium to non-equilibrium.** In (a), one can observe that the density of states  $A(\omega)$  of the electronic system exhibits two Hubbard peaks and an additional central peak at equilibrium (i.e., bias voltage  $\Phi = 0$ ). By increasing the bias voltage  $\Phi$  to non-equilibrium, the central peak is suppressed and splits into two. In (b), we show the effects of the Kondo resonance on the differential conductance as a function of bias voltage  $\Phi$ . The conductance  $G$  has a peak at  $\Phi = 0$  as the Kondo resonance acts as a transport channel for the electron.

the different contributions to the total Hamiltonian, as given in Equation (1), can be expressed as

$$\begin{aligned}
 H_s &= \varepsilon d^\dagger d + \omega_c a^\dagger a + g d^\dagger d (a + a^\dagger), \\
 H_f &= \sum_{\alpha=L,R} \sum_k \varepsilon_{\alpha,k} c_{\alpha,k}^\dagger c_{\alpha,k}, \\
 H_b &= \sum_k \omega_k b_k^\dagger b_k, \\
 H_{sf} &= \sum_{\alpha=L,R} \sum_k g_{\alpha,k} c_{\alpha,k}^\dagger d + g_{\alpha,k}^* d^\dagger c_{\alpha,k}, \\
 H_{sb} &= \sum_k g_k (a + a^\dagger) (b_k + b_k^\dagger),
 \end{aligned}$$

in terms of the energy  $\varepsilon$  of the electronic state, the frequency  $\omega_c$  of the single-mode cavity, the electron-cavity coupling strength  $g$ , and the annihilation (creation) operator  $a$  ( $a^\dagger$ ) of the single-mode cavity. We assume a Drude-Lorentz (Lorentzian) spectral density for the bosonic (fermionic) reservoir(s). As previously discussed, the correlation function in Equation (10) and Equation (11) can be expressed as a sum of exponential terms using the Padé decomposition, as shown in Equation (12) and Equation (13), respectively.

The environmental spectral densities depend on the following physical parameters: the coupling strength  $\Gamma_L = \Gamma_R = \Gamma$  between the electron and the fermionic reservoirs, the coupling strength  $\Delta$  between the single-mode cavity and the bosonic reservoir, the band-width  $W_\alpha$  ( $W_\beta$ ) of the fermionic (bosonic) reservoirs, the chemical potentials  $\mu_L = -\mu_R = \Phi/2$  for the left and right fermionic reservoirs, and the temperature  $T$  common to all reservoirs. All values of the parameters are summarized in Table. II. Using these parameters as input in `Heom.jl`, we can construct the HEOMLS matrix  $\hat{M}$  and solve for the stationary states of all the ADOs.

We now compute the spectra (see Methods) of both the charge (density of states; DOS) and cavity (power spectral density; PSD) using the built-in function in `Heom.jl`, and plot the results in Fig. 4. Here, we consider the bias voltage  $\Phi = 6$ , such that the site energy of the charge system aligns with the Fermi-level of one of the fermionic reservoirs, increasing the likelihood of electron tunneling to the fermionic reservoirs. We first discuss the DOS of the charge system, as shown in Fig. 4(a). As the coupling strength  $g$  between the charge and the cavity increases, the DOS of the charge system decreases and its peak shifts towards lower energies. This can be attributed to the energy shift induced by the cavity field on the electronic level.

To explore the charge-cavity interaction, we now analyze the PSD of the cavity system, see Fig. 4(b). The PSD of the cavity exhibits a single large peak at  $\omega = \Gamma = \omega_c$  for  $g \in (0, 0.5]$ , indicating that the cavity resonance is largely unaffected by the electronic system, but that it does induce additional broadening.

It is interesting to further compare the differences between the HEOM and a perturbative master equation (ME) approach. We do this by reducing the interaction strength  $\Delta = 0.01\omega_c$  between the cavity and its bosonic reservoir to a weak-coupling regime. We model the interaction between the system and bosonic reservoir with a Born-Markov master equation [41] using the Lindbladian given in Eq. (21). More specifically, we replace the bosonic part of HEOM with the following term

$$J_\beta(\omega_c) \left[ (n_\beta^{\text{eq}}(\omega_c) + 1) \hat{J}(a) + n_\beta^{\text{eq}}(\omega_c) \hat{J}(a^\dagger) \right] \rho_{|\mathbf{q}}^{(0,n,p)}(t) \quad (22)$$

on the right-hand side of Eq. (16). Here,  $J_\beta$  is the spectral density of the bosonic bath (assumed to be Drude-Lorentz in this case) and  $n_\beta^{\text{eq}}$  is the Bose-Einstein distribution. In this specific scenario, it is evident that the outcomes derived from the master equation approach may overestimate the magnitude when compared to the HEOM results in the high-frequency range of the PSD. The origin of this inconsistency can be attributed to the non-Markovian effect [5, 9, 82, 83] arising from the bosonic reservoir, characterized by the narrow band-width of the Drude-Lorentz spectral density ( $W_\beta = 0.2$ ) we use to describe it; even though the coupling strength is weak, this narrow width implies the environment can still have memory. In addition, the master equation has limited capability in addressing the combined influence of electron-cavity interactions and electron-fermionic-reservoir hybridization. Nevertheless, these challenges can be effectively tackled using the HEOM approach.

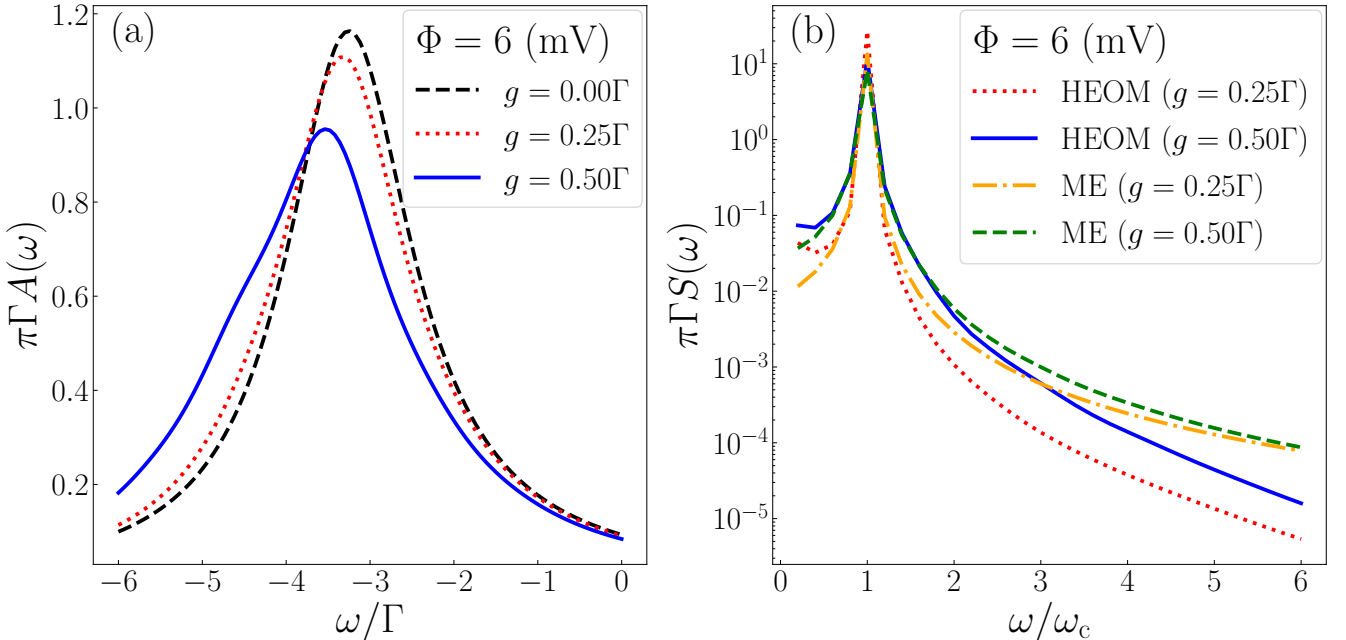


**Figure 4. Effects of the electron-cavity coupling on the spectra of the charge and cavity system.** In (a), the resonance in the density of states  $A(\omega)$  of the charge system is reduced and shifts towards lower energies as the charge-cavity coupling strength  $g$  increases. In (b), we plot the power spectral density  $S(\omega)$  of the cavity and uses two different methods (HEOM and ME) to describe the interaction between the cavity and the bosonic reservoir. Both approaches show a single peak at  $\omega = \Gamma$  for  $g \in (0, 0.5]$ . The Born-Markov approximation used to derive the ME may result in an inaccurate estimation of the magnitude of the  $S(\omega)$  compared to the HEOM, especially in the high-frequency range.

Applying the same methodology as in the previous example, one can also calculate the conductance between the charge system and the fermionic reservoirs, as shown in Fig. 5. We begin by examining the case when the charge system is not coupled to the cavity ( $g = 0$ ). In this scenario, due to the finite band-width of the fermionic reservoirs  $W_\alpha$  and a site energy of the charge system  $\epsilon = -3$  being far away from the Fermi-level, a local minimum of the conductance is observed at  $\Phi = 0$ . Additionally, the conductance increases with increasing  $|\Phi|$ , reaching its maximum value when the site energy  $\epsilon$  coincides with the Fermi-level of one of the fermionic reservoirs, resulting in the splitting of the peaks in the conductance.

Conversely, when the charge is coupled to the cavity ( $g > 0$ ), the average energy of the charge in the electronic system decreases away from the Fermi-levels of the fermionic reservoirs, resulting in a decrease in conductance. It should be noted that the maximum conductance will be achieved with larger  $|\Phi|$ , leading to a wider splitting of the conductance peak.

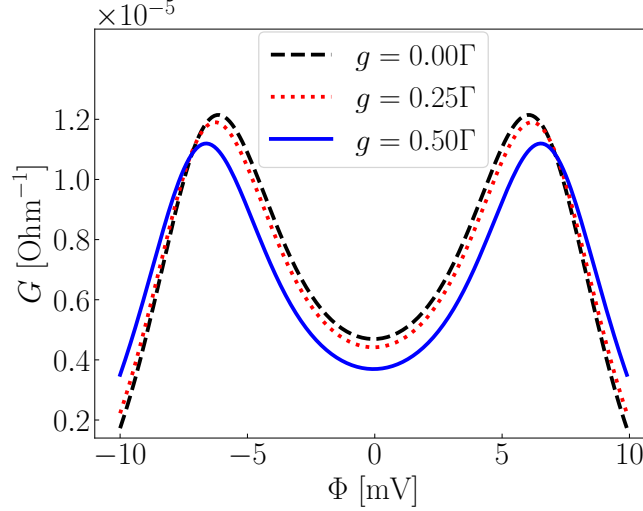


**Figure 5. Effect of the electron-cavity coupling on the conductance between the charge system and fermionic reservoirs.** The conductance  $G$  depends on the absolute value of the bias voltage  $\Phi$  and reaches its maximum when the average energy of the charge system is equal to the Fermi-level of one of the fermionic reservoirs, i.e., when  $e|\Phi|/2 = \varepsilon$ . As the electron-cavity coupling  $g$  increases, both the conductance  $G$  and the average energy of the charge system decrease, resulting in a wider splitting of the conductance peaks.

Package Name	PHI [57]	HEOM-QUICK [24]	DM-HEOM [58]	PyHEOM [59]	QuTiP-BoFiN [15]	Heom.jl
Language	Fortran	Fortran	C/C++	C++ / Python	Python	Julia
Documentation	✓	✓	✓	✗	✓	✓
RunTests	✗	✗	✗	✗	✓	✓
Bosonic Bath	✓	✗	✓	✓	✓	✓
Fermionic Bath	✗	✓	✗	✗	✓	✓
Hybrid Bath	✗	✗	✗	✗	✓	✓
T-D system support	✗	✓	✗	✗	✓	✓
Parity support	✗	✓	✗	✗	✗	✓
Importance support	✗	✗	✗	✗	✗	✓

**Table III. Comparison between different open source HEOM packages.** For each package, the check (cross) mark represents the presence (absence) of support for the listed functionalities. "Language" specifies the programming language. "Documentation" labels the availability of instructions for installing and running the code. "RunTests" describes the availability of a suite of tests to ensure the correct functionality of the package. "T-D system" describes the availability of the system Hamiltonian  $H_s$  to be time-dependent (T-D). "Parity" describes the availability of constructing the HEOMLS matrices within even- and odd-parity for fermionic baths.

#### Capabilities of Heom.jl and comparison with other packages

Recent developments in the field of HEOM have led to an explosion of open source software, such as PHI [57], HEOM-QUICK [24], DM-HEOM [58], PyHEOM [59], and QuTiP-BoFiN [15, 84, 85]. These packages are written in different programming languages which have different capabilities. Thus, in Table III, we briefly compare their differences and similarities with respect to Heom.jl.

We first emphasize the significance of specifying the importance threshold  $\mathcal{I}_{\text{th}}$  and estimating the importance for each ADOs with Eq. (20), which are not available for other packages listed in Table III. The main computational complexity can be quantified by the total number of ADOs because it directly affects the size of  $\hat{\mathcal{M}}$ . The importance criterion  $\mathcal{I}(\rho_{\mathbf{j}|\mathbf{q}}^{(m,n,p)}) \geq \mathcal{I}_{\text{th}}$  allows us to only consider the ADOs which affects the dynamics more, and thus, reduce the size of  $\hat{\mathcal{M}}$ . Table IV summarizes the number of ADOs with respect to different truncation level  $n_{\text{max}}$  and importance thresholds  $\mathcal{I}_{\text{th}}$ . Interestingly, it is possible to observe a significant reduction in the number of auxiliary density operators when  $\mathcal{I}_{\text{th}}$  increases.

We further discuss the consistency of the importance criterion and consider the parameter settings in example 1 (see Table II). In this case, we first increase the truncation level until we find out that the values of electronic current converges at  $n_{\text{max}} = 4$ ,

$n_{\max} \setminus \mathcal{I}_{\text{th}}$	$10^{-3}$	$10^{-4}$	$10^{-5}$	$10^{-6}$	$10^{-7}$	$10^{-8}$	$10^{-9}$	$10^{-10}$	0.0
1	57	57	57	57	57	57	57	57	57
2	249	873	1,193	1,421	1,569	1,597	1,597	1,597	1,597
3	305	1,489	4,241	12,713	18,933	23,693	27,161	28,645	29,317
4	305	1,489	5,011	18,901	49,713	126,715	205,803	274,249	396,607
5	305	1,489	5,011	19,013	55,173	170,297	418,589	931,551	4,216,423
6	305	1,489	5,011	19,013	55,201	171,557	444,979	1,137,239	36,684,859

**Table IV. Number of auxiliary density operators for different truncation values of the fermionic hierarchy level and different thresholds of the importance value.** Here, we use the parameters from example 1 (see Table II). Note that we only neglect the ADOs in the second and higher levels ( $n \geq 2$ ) whose importance value is smaller than  $\mathcal{I}_{\text{th}}$ .

which requires 396,607 ADOs (as shown in Table. IV) to describe the dynamics. The effects on the convergence of the electronic current while using the importance criterion are shown in Fig. 6. For the equilibrium case ( $\Phi = 0$ ), one can observe that the electronic current already converged at  $\mathcal{I}_{\text{th}} = 10^{-5}$ . However, by increasing the bias voltage to non-equilibrium  $\Phi > 0$ , the results obtained with a higher  $\mathcal{I}_{\text{th}}$  show larger deviation from the converged results. The results converge at  $\mathcal{I}_{\text{th}} = 10^{-7}$  and require only 49,713 ADOs (as shown in Table. IV). For too large thresholds  $\mathcal{I}_{\text{th}} \geq 10^{-4}$ , we observe unphysical negative electronic currents or even fail to obtain the stationary states of the ADOs.

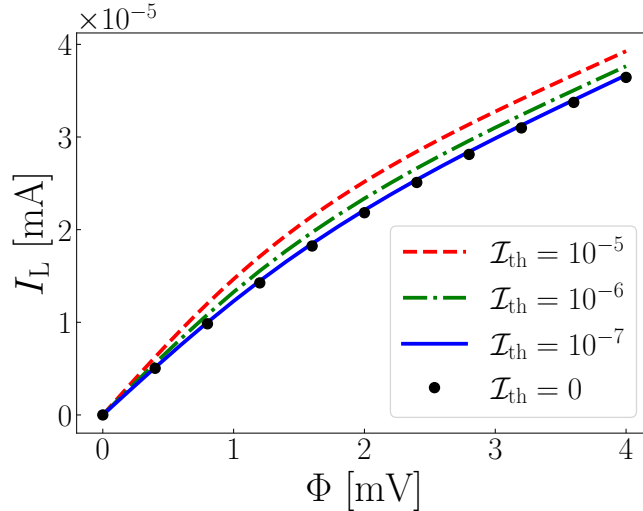


**Figure 6. Convergence of the electronic current with respect to the importance threshold.** Here, we consider the parameters setting in example 1 (see Table II) and show the electronic current  $I_L$  (from the left-hand side fermionic reservoir into the system) as a function of bias voltage  $\Phi$  with respect to the importance threshold  $\mathcal{I}_{\text{th}}$ . The values of electronic current converge when  $\mathcal{I}_{\text{th}} = 10^{-7}$ , which reduces the number of ADOs from 396,607 ( $\mathcal{I}_{\text{th}} = 0$ ) to 49,713, as shown in Table IV.

We now compare the performance in constructing HEOMLS matrix  $\hat{\mathcal{M}}$ , solving time evolution (TE) of ADOs and solving the stationary states (SS) of ADOs between `Heom.jl` and `QuTiP-BoFiN` [15, 84, 85]. This choice is motivated by the fact that `QuTiP-BoFiN` served as an inspiration and guide for the development of this package, and thus has similar features, and by the fact that they are both purely written in high-level languages (Python and Julia). For this comparison, we consider the same setting in example 1 (see Table II). The benchmark result of constructing  $\hat{\mathcal{M}}$  are shown in Fig. 7(a). `Heom.jl` not only improves the computational time on single-thread processing but also supports multi-threading to make the process of constructing  $\hat{\mathcal{M}}$  faster. Note that we only consider the importance threshold  $\mathcal{I}_{\text{th}} = 0.0$  in this benchmark because `QuTiP-BoFiN` does not support this functionality at this time. On top of the speed up in constructing  $\hat{\mathcal{M}}$ , we emphasize that `Heom.jl` is also faster in computing the time evolution and stationary states of the ADOs, as shown in Fig. 7(b), largely because of underlying performance benefits of the numerical libraries in Julia [40, 42, 43]. For example, `DifferentialEquations.jl` [42] provides a unified user interface to solve the differential equations with various choices of solver. `Heom.jl` wrapped a subset of the functions in `DifferentialEquations.jl` for solving TE of the ADOs, and users can optimize their solver choice depending on the problem. We have also wrapped some of the functions in `LinearSolver.jl` [40] for users to solve the

stationary states of ADOs and the spectrum of the system with different solvers. In our experience, these functionalities allow a significant improvement in both runtime and accuracy compared to the libraries currently available in Python.

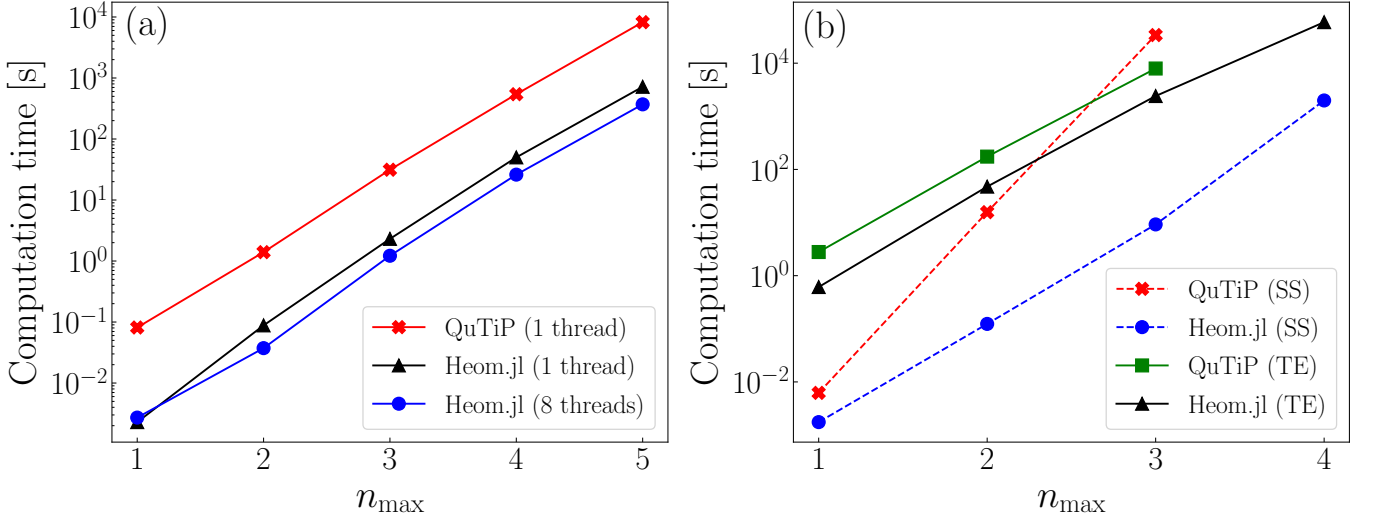


Figure 7. **Benchmark of the performance between Heom.jl and QuTiP-BoFiN.** We consider the parameters used in example 1 (see Table II). Note that QuTiP-BoFiN currently does not support the estimation of importance for ADOs, and thus, we set  $\mathcal{I}_{\text{th}} = 0$  here. The benchmark was done on a workstation with two Intel(R) Xeon(R) Silver 4110 @2.10GHz CPUs and 256 GB memory. The software versions were QuTiP 4.7.1, Heom.jl 0.1.0, Python 3.7.6, and Julia 1.8.2. The operating system was CentOS Linux 8.1.1911. In (a), we show the total runtime versus truncation level  $n_{\max}$  for the construction of the HEOMLS matrices  $\hat{M}$  using the corresponding packages. "x-threads" means that there are  $x$ -threads used during the process of constructing the matrices. Note that QuTiP-BoFiN currently only supports single-thread process for the construction of  $\hat{M}$ . In (b), we show the total runtime versus truncation level  $n_{\max}$  for calculating the stationary states (SS) and time evolution (TE) of the auxiliary density operators using the corresponding packages.

## CONCLUSION

In conclusion, the `Heom.jl` software package provides a user-friendly and efficient tool for simulating complex open quantum systems, including non-Markovian effects due to non-perturbative interaction with one, or multiple, environments. While integrating many of the features present in other open-source HEOM packages, `Heom.jl` also includes new functionalities, such as the estimation of importance values for all ADOs, the calculation of spectra for both bosonic and fermionic systems, and the construction of even- and odd-parity HEOMLS matrices for fermionic baths. By wrapping some functions from other `Julia` packages, we could further optimize the computation of the dynamics and stationary states for all ADOs.

We exemplified the functionalities of `Heom.jl` using two physics examples where we observed order of magnitudes speedups with respect to `QuTiP-BoFiN` in constructing HEOMLS matrices and solving dynamics and stationary states for all ADOs. As a result, we believe that `Heom.jl` will be a valuable tool for researchers working in different fields such as quantum biology, quantum optics, quantum thermodynamics, quantum information, quantum transport, and condensed matter physics.

We further plan to extend the software for future releases in two different directions. First, we aim to add fitting routines to the decomposition methods used to compute correlation functions, thereby expanding the domain of spectral densities supported by the HEOM approach. Second, we aim to improve the computational efficiency of the package by reducing the complexity of the HEOM (for example imposing Hermiticity [23, 24]) and by including support for distributed computing on clusters and GPU computing.

## METHODS

### Fermion correlation function with Lorentzian spectral density

In this subsection, we present an example for the decomposition of a  $\alpha$ -fermionic reservoir correlation function as a sum of  $N_\alpha$ -exponential terms. In particular, we focus on the following Lorentzian spectral density

$$J_\alpha(\omega) = \frac{\Gamma_\alpha W_\alpha^2}{(\omega - \mu_\alpha)^2 + W_\alpha^2}, \quad (23)$$

where  $\Gamma_\alpha$  represents the coupling strength between system and  $\alpha$ -fermionic reservoir with band-width  $W_\alpha$  and chemical potential  $\mu_\alpha$ . We now express the Fermi-Dirac distribution  $n_\alpha^{\text{eq}}(x) = \{\exp(x) + 1\}^{-1}$  as a series by employing the Padé decomposition [53] (which has been reported[15, 54] to enjoy a faster convergence than the Matsubara one [52]) to obtain

$$n_\alpha^{\text{eq}}(x) \approx n_\alpha^{\text{Padé}}(x) = \frac{1}{2} - \sum_{h=2}^{N_\alpha} \frac{2\kappa_h x}{x^2 + \zeta_h^2}, \quad (24)$$

where the parameters  $\kappa_h$  and  $\zeta_h$  are described in previous work [53] and depend on the choice of  $N_\alpha$ . Thus, the integration in Eq. (10) can be analytically performed using the residue theorem and results in Eq. (12), which explicitly reads

$$C_\alpha^v(\tau) \approx \sum_{h=1}^{N_\alpha} \eta_{\alpha,h}^v \exp(-\gamma_{\alpha,h}^v \tau) \quad (25)$$

with

$$\begin{aligned} \eta_{\alpha,1}^v &= \frac{\Gamma_\alpha W_\alpha}{2} n_\alpha^{\text{Padé}}\left(\frac{iW_\alpha}{k_B T}\right), \\ \gamma_{\alpha,1}^v &= W_\alpha - vi\mu_\alpha, \\ \eta_{\alpha,h \neq 1}^v &= -i\kappa_h k_B T \cdot \frac{\Gamma_\alpha W_\alpha^2}{-(\zeta_h k_B T)^2 + W_\alpha^2}, \\ \eta_{\alpha,h \neq 1}^v &= \zeta_h k_B T - vi\mu_\alpha. \end{aligned} \quad (26)$$

### Boson correlation function with Drude-Lorentz spectral density

In this subsection, we present an example for the decomposition of a  $\beta$ -bosonic reservoir correlation function as a sum of  $N_\beta$ -exponential terms. In particular, we focus on the following Drude-Lorentz spectral density

$$J_\beta(\omega) = \frac{4\pi\Delta_\beta W_\beta \omega}{\omega^2 + W_\beta^2}, \quad (27)$$

in which  $\Delta_\beta$  represents the coupling strength between the system and the  $\beta$ -bosonic reservoir with band-width  $W_\beta$ . Similarly as in the fermionic case, we can now express the Bose-Einstein distribution  $n_\beta^{\text{eq}}(x) = \{\exp(x) - 1\}^{-1}$  as a series by employing the Padé decomposition [53], to obtain

$$n_\beta^{\text{eq}}(x) \approx n_\beta^{\text{Padé}}(x) = \frac{1}{x} - \frac{1}{2} + \sum_{l=2}^{N_\beta} \frac{2\kappa_l x}{x^2 + \zeta_l^2}, \quad (28)$$

where the parameters  $\kappa_l$  and  $\zeta_l$  are described in previous work [53] and depend on the choice of  $N_\beta$ . Using this decomposition, the integration in Eq. (11) can be analytically performed using the residue theorem and results in Eq. (13), which explicitly reads

$$C_\beta(\tau) \approx \sum_{l=1}^{N_\beta} \xi_{\beta,l} \exp(-\chi_{\beta,l} \tau) \quad (29)$$

with

$$\begin{aligned}
\xi_{\beta,1} &= \Delta_\beta W_\beta \left( -i + \cot \left( \frac{W_\beta}{2k_B T} \right) \right), \\
\chi_{\beta,1} &= W_\beta, \\
\xi_{\beta,l \neq 1} &= -2\kappa_l k_B T \cdot \frac{2\Delta_\beta W_\beta \cdot \zeta_l k_B T}{-(\zeta_l k_B T)^2 + W_\beta^2}, \\
\chi_{\beta,l \neq 1} &= \zeta_l k_B T.
\end{aligned} \tag{30}$$

Contrary to the fermionic case, we note that, here, the correlation function does not have to be further decomposed into its real and imaginary part since  $\chi_{\beta,l} = \chi_{\beta,l}^* \forall l$ .

### Numerical computation of the spectrum

In this subsection, we briefly summarize how to numerically compute the spectrum associated with the system degree of freedom. Previous work [13] showed that the spectrum can be evaluated either in time or frequency domain. `Heom.jl` provides a built-in function which performs the calculation in frequency domain. In the following, we first focus on the bosonic case (to compute the power spectral density) and, next, on fermionic case (to compute the density of states).

In order to compute the power spectral density in the time-domain, we write the system correlation function in terms of the propagator  $\hat{G}(t) = \exp(\hat{\mathcal{M}}t)$ , for  $t > 0$ , when the system Hamiltonian is time-independent. The power spectral density associated with  $\sigma_b$  can be obtained as

$$\begin{aligned}
\pi S_{\sigma_b}(\omega) &= \text{Re} \left\{ \int_0^\infty dt \langle a_{\sigma_b}^\dagger(t) a_{\sigma_b}(0) \rangle^* e^{i\omega t} \right\} \\
&= \text{Re} \left\{ \int_0^\infty dt \langle a_{\sigma_b}^\dagger(t) a_{\sigma_b}(0) \rangle e^{-i\omega t} \right\} \\
&= \text{Re} \left\{ \int_0^\infty dt \langle a_{\sigma_b}^\dagger e^{\hat{\mathcal{M}}t} a_{\sigma_b} \rangle e^{-i\omega t} \right\} \\
&= \text{Re} \left\{ \int_0^\infty dt \langle a_{\sigma_b}^\dagger e^{(\hat{\mathcal{M}}-i\omega)t} a_{\sigma_b} \rangle \right\} \\
&= \text{Re} \left\{ -\langle a_{\sigma_b}^\dagger (\hat{\mathcal{M}}-i\omega)^{-1} a_{\sigma_b} \rangle \right\} \\
&= -\text{Re} \left\{ \text{Tr} \left[ a_{\sigma_b}^\dagger (\hat{\mathcal{M}}-i\omega)^{-1} a_{\sigma_b} \rho_{\mathbf{j}|\mathbf{q}}^{(m,n,+)} \right] \right\} \\
&= -\text{Re} \left\{ \text{Tr} \left[ a_{\sigma_b}^\dagger \mathbf{x} \right] \right\},
\end{aligned} \tag{31}$$

where a half-Fourier transform has been introduced in the fifth line. To determine  $\mathbf{x}$  at a fixed frequency  $\omega$ , one can express all of the ADOs in a vector form and then solve the linear problem  $\mathbf{Ax} = \mathbf{b}$  (where  $\mathbf{A} = \hat{\mathcal{M}} - i\omega$  and  $\mathbf{b} = a_{\sigma_b} \rho_{\mathbf{j}|\mathbf{q}}^{(m,n,+)}$ ) using the package `LinearSolve.jl` [40]. We note that, while in principle all the ADOs are required to solve for  $\mathbf{x}$ , only the reduced density operator ( $m = 0$  and  $n = 0$ ) is considered when taking the final trace.

In order to compute the density of states, we start from the retarded Green's function [13]

$$G_{\sigma_f}^R(t) = -i\Theta(t) \left\{ \langle d_{\sigma_f}(t) d_{\sigma_f}^\dagger(0) \rangle + \langle d_{\sigma_f}^\dagger(t) d_{\sigma_f}(0) \rangle^* \right\}, \tag{32}$$

in which the Heaviside function  $\Theta(t)$  is needed to impose causality. Similarly to the bosonic case, the density of states associated with  $\sigma_f$  can be written in compact form as

$$\begin{aligned}
\pi A_{\sigma_f}(\omega) &= -\text{Im} \int_{-\infty}^\infty G_{\sigma_f}^R(t) e^{i\omega t} dt \\
&= \text{Re} \left\{ \int_0^\infty dt \left[ \langle d_{\sigma_f}(t) d_{\sigma_f}^\dagger(0) \rangle + \langle d_{\sigma_f}^\dagger(t) d_{\sigma_f}(0) \rangle^* \right] e^{i\omega t} \right\} \\
&= -\text{Re} \left\{ \text{Tr} \left[ d_{\sigma_f} (\hat{\mathcal{M}} + i\omega)^{-1} d_{\sigma_f}^\dagger \rho_{\mathbf{j}|\mathbf{q}}^{(m,n,+)} \right] + \text{Tr} \left[ d_{\sigma_f}^\dagger (\hat{\mathcal{M}} - i\omega)^{-1} d_{\sigma_f} \rho_{\mathbf{j}|\mathbf{q}}^{(m,n,+)} \right] \right\} \\
&= -\text{Re} \left\{ \text{Tr} \left[ d_{\sigma_f} \mathbf{x}_+ \right] + \text{Tr} \left[ d_{\sigma_f}^\dagger \mathbf{x}_- \right] \right\},
\end{aligned} \tag{33}$$

where  $\mathbf{x}_+$  is determined by solving

$$(\hat{\mathcal{M}} + i\omega)\mathbf{x}_+ = d_{\sigma_f}^\dagger \rho_{\mathbf{j}|\mathbf{q}}^{(m,n,+)}, \quad (34)$$

and  $\mathbf{x}_-$  is determined by solving

$$(\hat{\mathcal{M}} - i\omega)\mathbf{x}_- = d_{\sigma_f} \rho_{\mathbf{j}|\mathbf{q}}^{(m,n,+)}. \quad (35)$$

Here, the HEOMLS matrix  $\hat{\mathcal{M}}$  acts on the odd-parity ( $p = -$ ) space, compatibly with the parity of both the operators  $d_{\sigma_f} \rho_{\mathbf{j}|\mathbf{q}}^{(m,n,+)}$  and  $d_{\sigma_f}^\dagger \rho_{\mathbf{j}|\mathbf{q}}^{(m,n,+)}$ . As for the computation of the power spectral density, we only need the reduced density operator ( $m = 0$  and  $n = 0$ ) to take the final trace operation.

### Electronic Current

In this subsection, we discuss how to compute an environmental observable: the electronic current. Within the influence functional approach [21, 23], the expectation value of the electronic current from the  $\alpha$ -fermionic bath into the system can be written in terms of the first-level-fermionic ( $n = 1$ ) auxiliary density operators, namely

$$\begin{aligned} \langle I_\alpha(t) \rangle &= (-e) \frac{d\langle \mathcal{N}_\alpha \rangle}{dt} \\ &= ie \sum_{v,h,\sigma_f} (-1)^{\delta_{v,-}} \text{Tr} \left[ d_{\sigma_f}^v \rho_{\{\alpha,v,h,\sigma_f\}}^{(0,1,+)}(t) \right], \end{aligned} \quad (36)$$

where  $e$  represents the value of the elementary charge, and  $\mathcal{N}_\alpha = \sum_k c_{\alpha,k}^\dagger c_{\alpha,k}$  is the occupation number operator for the  $\alpha$ -fermionic bath. To compute this quantity, it is possible to first use `Heom.jl` to obtain the stationary states for the ADOs  $\rho_{\mathbf{j}|\mathbf{q}}^{(m,n,+)}(t)$ , and then use the hierarchy dictionary [as shown in Fig. 1(e)] to identify all the zeroth-level-bosonic-and-first-level-fermionic ( $m = 0$  and  $n = 1$ ) ADOs and their corresponding indices  $\alpha$ ,  $v$ ,  $h$ , and  $\sigma_f$  to be used in Eq. (36).

### CODE AVAILABILITY

The `Heom.jl` package is available through a public GitHub repo (<https://github.com/NCKU-QFort/Heom.jl>). It is also registered in the `Julia` package registry and can be installed by the `Julia` package manager. Moreover, detailed information (documentation and examples) is available through a public website (<https://ncku-qfort.github.io/Heom.jl>).

### ACKNOWLEDGEMENTS

The authors acknowledge fruitful discussions with Yuan-Ching Lin and Chung-Hsuan Tung. N.L. acknowledges partial support from JST PRESTO through Grant No. JPMJPR18GC, and the Information Systems Division, RIKEN, for the use of their facilities. M.C. acknowledges support from NSFC (Grants No. 12050410264 and No. 11935012) and NSAF (Grant No. U1930403). F.N. is supported in part by: Nippon Telegraph and Telephone Corporation (NTT) Research, the Japan Science and Technology Agency (JST) [via the Quantum Leap Flagship Program (Q-LEAP), and the Moonshot R&D Grant Number JP-MJMS2061], and the Asian Office of Aerospace Research and Development (AOARD) (via Grant No. FA2386-20-1-4069). F.N. and N.L. acknowledge the Foundational Questions Institute Fund (FQXi) via Grant No. FQXi-IAF19-06. YNC acknowledges the support of the National Science and Technology Council, Taiwan (MOST Grants No. 111-2123-M-006-001).

---

[1] R. Zwanzig, Ensemble method in the theory of irreversibility, *The Journal of Chemical Physics* **33**, 1338 (1960).  
[2] R. Feynman and F. Vernon, The theory of a general quantum system interacting with a linear dissipative system, *Ann. Phys.* **24**, 118 (1963).  
[3] A. Caldeira and A. Leggett, Path integral approach to quantum Brownian motion, *Physica A* **121**, 587 (1983).  
[4] P. Hedegård and A. O. Caldeira, Quantum dynamics of a particle in a Fermionic environment, *Phys. Scripta* **35**, 609 (1987).

- [5] H.-B. Chen, N. Lambert, Y.-C. Cheng, Y.-N. Chen, and F. Nori, Using non-Markovian measures to evaluate quantum master equations for photosynthesis, *Sci. Rep.* **5**, 12753 (2015).
- [6] Y. Tanimura and R. Kubo, Time evolution of a quantum system in contact with a nearly Gaussian-Markoffian noise bath, *J. Phys. Soc. Jpn.* **58**, 101 (1989).
- [7] Y. Tanimura, Nonperturbative expansion method for a quantum system coupled to a harmonic-oscillator bath, *Phys. Rev. A* **41**, 6676 (1990).
- [8] R. Bulla, T. A. Costi, and T. Pruschke, Numerical renormalization group method for quantum impurity systems, *Rev. Mod. Phys.* **80**, 395 (2008).
- [9] W.-M. Zhang, P.-Y. Lo, H.-N. Xiong, M. W.-Y. Tu, and F. Nori, General non-Markovian dynamics of open quantum systems, *Phys. Rev. Lett.* **109**, 170402 (2012).
- [10] P. Strasberg, G. Schaller, N. Lambert, and T. Brandes, Nonequilibrium thermodynamics in the strong coupling and non-Markovian regime based on a reaction coordinate mapping, *New J. Phys.* **18**, 073007 (2016).
- [11] M. Brenes, J. J. Mendoza-Arenas, A. Purkayastha, M. T. Mitchison, S. R. Clark, and J. Goold, Tensor-network method to simulate strongly interacting quantum thermal machines, *Phys. Rev. X* **10**, 031040 (2020).
- [12] J. K. Sowa, N. Lambert, T. Seideman, and E. M. Gauger, Beyond Marcus theory and the Landauer–Büttiker approach in molecular junctions. II. A self-consistent Born approach, *J. Chem. Phys.* **152**, 064103 (2020).
- [13] Z. Li, N. Tong, X. Zheng, D. Hou, J. Wei, J. Hu, and Y. Yan, Hierarchical Liouville-space approach for accurate and universal characterization of quantum impurity systems, *Phys. Rev. Lett.* **109**, 266403 (2012).
- [14] Y. Tanimura, Numerically “exact” approach to open quantum dynamics: The hierarchical equations of motion (HEOM), *J. Chem. Phys.* **153**, 020901 (2020).
- [15] N. Lambert, T. Raheja, S. Cross, P. Menczel, S. Ahmed, A. Pitchford, D. Burgarth, and F. Nori, Qutip-bofin: A bosonic and fermionic numerical hierarchical-equations-of-motion library with applications in light-harvesting, quantum control, and single-molecule electronics, *Phys. Rev. Res.* **5**, 013181 (2023).
- [16] N. Lambert, S. Ahmed, M. Cirio, and F. Nori, Modelling the ultra-strongly coupled spin-boson model with unphysical modes, *Nat. Commun.* **10**, 3721 (2019).
- [17] T. P. Fay and D. T. Limmer, Coupled charge and energy transfer dynamics in light harvesting complexes from a hybrid hierarchical equations of motion approach, *The Journal of Chemical Physics* **157**, 174104 (2022), <https://doi.org/10.1063/5.0117659>.
- [18] J. Ma, Z. Sun, X. Wang, and F. Nori, Entanglement dynamics of two qubits in a common bath, *Phys. Rev. A* **85**, 062323 (2012).
- [19] A. Kato and Y. Tanimura, Quantum heat current under non-perturbative and non-Markovian conditions: Applications to heat machines, *J. Chem. Phys.* **145**, 224105 (2016).
- [20] X.-Y. Chen, N.-N. Zhang, W.-T. He, X.-Y. Kong, M.-J. Tao, F.-G. Deng, Q. Ai, and G.-L. Long, Global correlation and local information flows in controllable non-Markovian open quantum dynamics, *npj Quantum Information* **8**, 22 (2022).
- [21] J. Jin, X. Zheng, and Y. Yan, Exact dynamics of dissipative electronic systems and quantum transport: Hierarchical equations of motion approach, *J. Chem. Phys.* **128**, 234703 (2008).
- [22] A. Ishizaki and G. R. Fleming, Unified treatment of quantum coherent and incoherent hopping dynamics in electronic energy transfer: Reduced hierarchy equation approach, *J. Chem. Phys.* **130**, 234111 (2009).
- [23] R. Härtle, G. Cohen, D. R. Reichman, and A. J. Millis, Decoherence and lead-induced interdot coupling in nonequilibrium electron transport through interacting quantum dots: A hierarchical quantum master equation approach, *Phys. Rev. B* **88**, 235426 (2013).
- [24] L. Ye, X. Wang, D. Hou, R.-X. Xu, X. Zheng, and Y. Yan, HEOM-quick: a program for accurate, efficient, and universal characterization of strongly correlated quantum impurity systems, *WIREs Computational Molecular Science* **6**, 608 (2016).
- [25] C. Schinabeck, R. Härtle, and M. Thoss, Hierarchical quantum master equation approach to electronic-vibrational coupling in nonequilibrium transport through nanosystems: Reservoir formulation and application to vibrational instabilities, *Phys. Rev. B* **97**, 235429 (2018).
- [26] J. Bätge, Y. Ke, C. Kaspar, and M. Thoss, Nonequilibrium open quantum systems with multiple bosonic and fermionic environments: A hierarchical equations of motion approach, *Phys. Rev. B* **103**, 235413 (2021).
- [27] J. Bezanson, S. Karpinski, V. B. Shah, and A. Edelman, Julia: A fast dynamic language for technical computing, arXiv preprint arXiv:1209.5145 (2012).
- [28] J. Bezanson, A. Edelman, S. Karpinski, and V. B. Shah, Julia: A fresh approach to numerical computing, *SIAM Review* **59**, 65 (2017).
- [29] B. W. Kernighan and D. M. Ritchie, *The C programming language* (Prentice Hall Professional Technical Reference, 2006).
- [30] D. Flanagan and Y. Matsumoto, *The Ruby Programming Language* (O'Reilly Media, Inc., 2007).
- [31] G. Van Rossum and F. L. Drake, *Python 3 Reference Manual* (CreateSpace, Scotts Valley, CA, 2009).
- [32] R Core Team, *R: A Language and Environment for Statistical Computing* (R Foundation for Statistical Computing, Vienna, Austria, 2021).
- [33] D. J. Higham and N. J. Higham, *MATLAB Guide* (Society for Industrial and Applied Mathematics, Philadelphia, PA, USA, 2017) pp. xxvi+476.
- [34] C. Lattner and V. Adve, LLVM: a compilation framework for lifelong program analysis & transformation, in *International Symposium on Code Generation and Optimization, 2004. CGO 2004.* (2004) p. 75.
- [35] H. Chen and D. A. Lidar, Hamiltonian open quantum system toolkit, *Communications Physics* **5**, 112 (2022).
- [36] S. Krämer, D. Plankensteiner, L. Ostermann, and H. Ritsch, QuantumOptics.jl: A Julia framework for simulating open quantum systems, *Computer Physics Communications* **227**, 109 (2018).
- [37] X.-Z. Luo, J.-G. Liu, P. Zhang, and L. Wang, Yao.jl: Extensible, Efficient Framework for Quantum Algorithm Design, *Quantum* **4**, 341 (2020).
- [38] P. Gawron, D. Kurzyk, and Ł. Pawela, QuantumInformation.jl—a Julia package for numerical computation in quantum information theory, *PLOS ONE* **13**, e0209358 (2018).

[39] J. Bätge, Y. Ke, C. Kaspar, and M. Thoss, Nonequilibrium open quantum systems with multiple bosonic and fermionic environments: A hierarchical equations of motion approach, *Phys. Rev. B* **103**, 235413 (2021).

[40] C. R. Will Kimmerer, Vedant Puri, [Linearsolve.jl](#).

[41] H.-P. Breuer and F. Petruccione, *The Theory of Open Quantum Systems* (Oxford University Press, 2007).

[42] C. Rackauckas and Q. Nie, DifferentialEquations.jl – a performant and feature-rich ecosystem for solving differential equations in Julia, *Journal of Open Research Software* **5**, 15 (2017).

[43] H. Hogben, M. Krzstyniak, G. Charnock, P. Hore, and I. Kuprov, Spinach – a software library for simulation of spin dynamics in large spin systems, *Journal of Magnetic Resonance* **208**, 179 (2011).

[44] M. Cirio, S. De Liberato, N. Lambert, and F. Nori, Ground state electroluminescence, *Phys. Rev. Lett.* **116**, 113601 (2016).

[45] A. Stockklauser, P. Scarlino, J. V. Koski, S. Gasparinetti, C. K. Andersen, C. Reichl, W. Wegscheider, T. Ihn, K. Ensslin, and A. Wallraff, Strong coupling cavity QED with gate-defined double quantum dots enabled by a high impedance resonator, *Phys. Rev. X* **7**, 011030 (2017).

[46] M. V. Gustafsson, T. Aref, A. F. Kockum, M. K. Ekström, G. Johansson, and P. Delsing, Propagating phonons coupled to an artificial atom, *Science* **346**, 207 (2014).

[47] R. Manenti, A. F. Kockum, A. Patterson, T. Behrle, J. Rahamim, G. Tancredi, F. Nori, and P. J. Leek, Circuit quantum acoustodynamics with surface acoustic waves, *Nat. Commun.* **8**, 975 (2017).

[48] I. Iorsh, A. Poshakinskiy, and A. Poddubny, Waveguide quantum optomechanics: Parity-time phase transitions in ultrastrong coupling regime, *Phys. Rev. Lett.* **125**, 183601 (2020).

[49] F. Benz, M. K. Schmidt, A. Dreismann, R. Chikkaraddy, Y. Zhang, A. Demetriadou, C. Carnegie, H. Ohadi, B. de Nijs, R. Esteban, J. Aizpurua, and J. J. Baumberg, Single-molecule optomechanics in “picocavities”, *Science* **354**, 726 (2016).

[50] P. C. Kuo, N. Lambert, A. Miranowicz, H. B. Chen, G. Y. Chen, Y. N. Chen, and F. Nori, Collectively induced exceptional points of quantum emitters coupled to nanoparticle surface plasmons, *Phys. Rev. A* **101**, 013814 (2020).

[51] M. Cirio, P. C. Kuo, Y. N. Chen, F. Nori, and N. Lambert, Canonical derivation of the fermionic influence superoperator, *Phys. Rev. B* **105**, 035121 (2022).

[52] Q. Shi, L. Chen, G. Nan, R.-X. Xu, and Y. Yan, Efficient hierarchical liouville space propagator to quantum dissipative dynamics, *The Journal of Chemical Physics* **130**, 084105 (2009), <https://doi.org/10.1063/1.3077918>.

[53] J. Hu, M. Luo, F. Jiang, R.-X. Xu, and Y. Yan, Padé spectrum decompositions of quantum distribution functions and optimal hierarchical equations of motion construction for quantum open systems, *J. Chem. Phys.* **134**, 244106 (2011), <https://doi.org/10.1063/1.3602466>.

[54] P.-C. Kuo, N. Lambert, M. Cirio, Y.-T. Huang, F. Nori, and Y.-N. Chen, The Kondo effect and photon trapping in a two-impurity anderson model ultra-strongly coupled to light, arXiv preprint arXiv:2302.01044 (2023).

[55] S. Wenderoth, J. Bätge, and R. Härtle, Sharp peaks in the conductance of a double quantum dot and a quantum-dot spin valve at high temperatures: A hierarchical quantum master equation approach, *Phys. Rev. B* **94**, 121303 (2016).

[56] R. Härtle, G. Cohen, D. R. Reichman, and A. J. Millis, Transport through an Anderson impurity: Current ringing, nonlinear magnetization, and a direct comparison of continuous-time quantum monte carlo and hierarchical quantum master equations, *Phys. Rev. B* **92**, 085430 (2015).

[57] J. Strümpfer and K. Schulten, Open quantum dynamics calculations with the hierarchy equations of motion on parallel computers, *Journal of Chemical Theory and Computation* **8**, 2808 (2012).

[58] T. Kramer, M. Noack, A. Reinefeld, M. Rodríguez, and Y. Zelinskyy, Efficient calculation of open quantum system dynamics and time-resolved spectroscopy with distributed memory HEOM (DM-HEOM), *Journal of Computational Chemistry* **39**, 1779 (2018).

[59] T. Ikeda and G. D. Scholes, Generalization of the hierarchical equations of motion theory for efficient calculations with arbitrary correlation functions, *The Journal of Chemical Physics* **152**, 204101 (2020).

[60] K. A. Velizhanin, H. Wang, and M. Thoss, Heat transport through model molecular junctions: A multilayer multiconfiguration time-dependent hartree approach, *Chemical Physics Letters* **460**, 325 (2008).

[61] A. Kato and Y. Tanimura, Quantum heat transport of a two-qubit system: Interplay between system-bath coherence and qubit-qubit coherence, *The Journal of Chemical Physics* **143**, 064107 (2015).

[62] L. Song and Q. Shi, Hierarchical equations of motion method applied to nonequilibrium heat transport in model molecular junctions: Transient heat current and high-order moments of the current operator, *Phys. Rev. B* **95**, 064308 (2017).

[63] D. Sprinzak, Y. Ji, M. Heiblum, D. Mahalu, and H. Shtrikman, Charge distribution in a Kondo-correlated quantum dot, *Phys. Rev. Lett.* **88**, 176805 (2002).

[64] A. J. Keller, S. Amasha, I. Weymann, C. P. Moca, I. G. Rau, J. A. Katine, H. Shtrikman, G. Zaránd, and D. Goldhaber-Gordon, Emergent SU(4) Kondo physics in a spin-charge-entangled double quantum dot, *Nat. Phys.* **10**, 145 (2013).

[65] K. Le Hur, Quantum dots and the Kondo effect, *Nature* **526**, 203 (2015).

[66] J. Park, A. N. Pasupathy, J. I. Goldsmith, C. Chang, Y. Yaish, J. R. Petta, M. Rinkoski, J. P. Sethna, H. D. Abruña, P. L. McEuen, and D. C. Ralph, Coulomb blockade and the Kondo effect in single-atom transistors, *Nature* **417**, 722 (2002).

[67] N. S. Wingreen, Quantum many-body effects in a single-electron transistor, *Science* **304**, 1258 (2004).

[68] L. H. Yu, Z. K. Keane, J. W. Ciszek, L. Cheng, M. P. Stewart, J. M. Tour, and D. Natelson, Inelastic electron tunneling via molecular vibrations in single-molecule transistors, *Phys. Rev. Lett.* **93**, 266802 (2004).

[69] A. Smith, M. S. Kim, F. Pollmann, and J. Knolle, Simulating quantum many-body dynamics on a current digital quantum computer, *npj Quantum Inf.* **5**, 106 (2019).

[70] S. Wang, X. Zheng, J. Jin, and Y. Yan, Hierarchical Liouville-space approach to nonequilibrium dynamical properties of quantum impurity systems, *Phys. Rev. B* **88**, 035129 (2013).

[71] L. Kouwenhoven and L. Glazman, Revival of the Kondo effect, *Physics World* **14**, 33 (2001).

[72] I. V. Borzenets, J. Shim, J. C. H. Chen, A. Ludwig, A. D. Wieck, S. Tarucha, H.-S. Sim, and M. Yamamoto, Observation of the Kondo screening cloud, *Nature* **579**, 210 (2020).

- [73] L. W. Smith, H.-B. Chen, C.-W. Chang, C.-W. Wu, S.-T. Lo, S.-H. Chao, I. Farrer, H. E. Beere, J. P. Griffiths, G. A. C. Jones, D. A. Ritchie, Y.-N. Chen, and T.-M. Chen, Electrically controllable kondo correlation in spin-orbit-coupled quantum point contacts, *Phys. Rev. Lett.* **128**, 027701 (2022).
- [74] W. G. van der Wiel, S. De Franceschi, J. M. Elzerman, T. Fujisawa, S. Tarucha, and L. P. Kouwenhoven, Electron transport through double quantum dots, *Rev. Mod. Phys.* **75**, 1 (2002).
- [75] L. E. Bruhat, T. Cubaynes, J. J. Viennot, M. C. Dartailh, M. M. Desjardins, A. Cottet, and T. Kontos, Circuit QED with a quantum-dot charge qubit dressed by Cooper pairs, *Phys. Rev. B* **98**, 155313 (2018).
- [76] D. J. van Woerkom, P. Scarlino, J. H. Ungerer, C. Müller, J. V. Koski, A. J. Landig, C. Reichl, W. Wegscheider, T. Ihn, K. Ensslin, and A. Wallraff, Microwave photon-mediated interactions between semiconductor qubits, *Phys. Rev. X* **8**, 041018 (2018).
- [77] P. Scarlino, D. J. van Woerkom, U. C. Mendes, J. V. Koski, A. J. Landig, C. K. Andersen, S. Gasparinetti, C. Reichl, W. Wegscheider, K. Ensslin, T. Ihn, A. Blais, and A. Wallraff, Coherent microwave-photon-mediated coupling between a semiconductor and a superconducting qubit, *Nat. Commun* **10**, 3011 (2019).
- [78] J. J. Viennot, M. R. Delbecq, M. C. Dartailh, A. Cottet, and T. Kontos, Out-of-equilibrium charge dynamics in a hybrid circuit quantum electrodynamics architecture, *Phys. Rev. B* **89**, 165404 (2014).
- [79] L. E. Bruhat, J. J. Viennot, M. C. Dartailh, M. M. Desjardins, T. Kontos, and A. Cottet, Cavity photons as a probe for charge relaxation resistance and photon emission in a quantum dot coupled to normal and superconducting continua, *Phys. Rev. X* **6**, 021014 (2016).
- [80] J. R. Souquet, M. J. Woolley, J. Gabelli, P. Simon, and A. A. Clerk, Photon-assisted tunnelling with nonclassical light, *Nature Communications* **5**, 5562 (2014).
- [81] A. F. Kockum, A. Miranowicz, S. D. Liberato, S. Savasta, and F. Nori, Publisher correction: Ultrastrong coupling between light and matter, *Nature Reviews Physics* **1**, 295 (2019).
- [82] Y.-N. Chen, G.-Y. Chen, Y.-Y. Liao, N. Lambert, and F. Nori, Detecting non-Markovian plasmonic band gaps in quantum dots using electron transport, *Phys. Rev. B* **79**, 245312 (2009).
- [83] H.-N. Xiong, P.-Y. Lo, W.-M. Zhang, D. H. Feng, and F. Nori, Non-Markovian complexity in the quantum-to-classical transition, *Scientific Reports* **5**, 13353 (2015).
- [84] J. Johansson, P. Nation, and F. Nori, QuTiP: An open-source Python framework for the dynamics of open quantum systems, *Computer Physics Communications* **183**, 1760 (2012).
- [85] J. Johansson, P. Nation, and F. Nori, QuTiP 2: A Python framework for the dynamics of open quantum systems, *Computer Physics Communications* **184**, 1234 (2013).